

ENHANCING SURFACE CHARACTERISTICS OF AA2024-T3 AIRCRAFT ALLOY THROUGH SYNERGISTIC ANODIZATION AND CERIUM CONVERSION COATING. PART II: MODIFICATION OF SURFACE PROPERTIES AND TOPOLOGY

Stefania Portolesi¹, Stephan Kozhukharov^{2,4}, Christian Girginov³,
Vanya Lilova⁴, Plamen Petkov⁴

¹University of Calabria, Via Pietro Bucci

87036 Arcavacata CS, Italy, stefania.portolesi@live.com

²LAMAR Laboratory, University of Chemical Technology and Metallurgy

8 Kliment Ohridski Blvd., Sofia 1797, Bulgaria, s.kozhukharov@uctm.edu (S.K.)

³Department of Physical Chemistry, University of Chemical Technology and Metallurgy

8 Kliment Ohridski Blvd., Sofia 1797, Bulgaria, girginov@uctm.edu (Ch.G.)

⁴Department of Physics, University of Chemical Technology and Metallurgy

8 Kliment Ohridski Blvd., Sofia 1797, Bulgaria, vanya.di@uctm.edu (V.L.), p.petkov@uctm.edu (P.P.)

Received 15 March 2024

Accepted 26 October 2024

DOI: 10.59957/jctm.v60.i1.2025.7

ABSTRACT

The present research is dedicated to the systematic characterization of the surface characteristics of AA2024-T3 specimens, after the formation of Anodic Aluminium Oxide (AAO) layer, deposition of a Cerium Conversion Coating (CeCC) and combination of these methods. The latter procedure was performed at two temperatures (20°C and 50°C). The investigations comprised combined AAO/CeCC coating primers, as well. All the obtained protective layers were subjected to systematic evaluations for determination of their colour characteristics, wettability and topology. The latter, including the layer thickness, was observed by both Optical Metallographic (OMM) and Scanning Electron (SEM) Microscopy. The outcome analysis of this study provides an additional contribution to the contemporary discussion on the formation of combined AAO/CeCC coating primers.

Keywords: AA2024-T3, anodization, cerium conversion coatings, surface properties, topology.

INTRODUCTION

Anodization of aluminium and its alloys is a well-known technological approach for the growth of highly-ordered anodic aluminium oxide (AAO) layers having uniform thickness. Their formation mechanism is an object of theoretical research since the mid-20th century. According to Abdel-Karim et al., the first concepts are introduced by Bauman (1939), followed by Keller (1953), Akahori (1961) and others [1]. All these classical views postulate that pore formation initiates after the formation of the barrier AAO layer is complete (Stage 1). Afterwards, pore initiation occurs because of local dissolution (Stage 2) of the already formed AAO. This process is followed by intensive oxide dissolution inside the already formed pores (Stage 3). Further, the

increased current density inside the pores causes local temperature increment which additionally enhances the dissolution. As a result, a steady-state growth of a porous oxide layer is established (Stage 4).

The structure characteristics of the basic porous AAO layer are summarized in a previous recent extended paper presented by Girginov et al., as follows: (i) pore diameter; (ii) interpore distance; (iii) pore depth, (iv) thickness of the barrier layer and (v) thickness of the entire porous AAO layer [2].

These structural characteristics are strongly dependent on the parameters of the anodization process: (i) applied electric regime (galvanostatic, potentiostatic, mixed, pulse, etc.); (ii) applied current density or voltage; (iii) nature of the contact electrolyte (mineral or organic acid); (iv) presence of additives in the electrolyte; (v)

process temperature; (vi) process duration and (vii) exact Al-alloy composition.

The influence of each of these factors is investigated in detail and is summarized in various extended theoretical works [3 - 8]. In turn, the topology, thickness and structure of the AAO layer predetermine its surface properties, such as: colour characteristics [9], corrosion protective abilities [10] and others. Hence, the multitude of factors, influencing the kinetics and mechanism of the anodization process determine the continuous interest towards this technique, as evident in recent research [10 - 15] and review [16, 17] papers.

On the other hand, the advantages of the Cerium Conversion Coatings (CeCC), as successful environmentally acceptable substitutes of the widely used Chromium Conversion Coatings (CCC) were recently emphasized [18, 19]. The basic concepts concerning the use of cerium compounds to effectively mitigate corrosion on metals by inhibition and formation of conversion coatings were postulated by the pioneering works of Hinton et al. in the mid-1980s [20, 21], followed by Davenport et al. [22, 23] and Mansfeld et al. [24, 25] in the early 1990s. The theoretical foundations regarding the formation of such type of corrosion protective films were further extended by Aldykiewicz et al. [26], Bethencourt et al. [27], Yasakau et al. [28], Conde et al. [29], Palomino et al. [30], Selegård et al. [31], Andreeva et al. [32, 33] and other authors.

In this sense, special attention to the great importance of the preliminary treatment of Al-based alloys, prior to the actual CeCC deposition is paid by de Frutos et al. [34] and Ping et al. [35]. Subsequently, the application of the anodization process to form a porous AAO matrix suitable for the deposition of a CeCC layer appeared as a rather interesting research object.

The objective of the present research is to determine in what way anodization and deposition of CeCC on AA2024-T3 alloy alter the surface properties and the performance in a model corrosive medium. In this sense, systematic comparative investigations were performed. To assess the influence of the temperature, the CeCC depositions were performed at 20°C, as well as at 50°C. The measurement techniques used were divided into two groups: (i) determination of surface properties (colour characteristics, wettability); (ii) topology characterization. The combined AAO/CeCC layers were subjected to further, more detailed characterization by

means of SEM and EDX mapping analyses. The adopted approach has facilitated the development of a conceptual model that explores the influence of both individual surface treatment procedures and their combined effects.

EXPERIMENTAL

Surface treatment procedures

Six pairs of plates (30x30x2 mm) cut from AA2024 were submitted to various combinations of surface treatments under the following conditions:

Preliminary treatment: This treatment was performed by immersing the samples in a 50 g dm⁻³ NaOH solution at 50°C for 2 min, followed by subsequent vigorous rinsing with both tap and distilled water. This procedure was succeeded by desmutting in diluted with distilled water HNO₃ (dilution ratio was 1:1) for 2 min at room temperature. Finally, the samples were again washed with tap and distilled water for about 1 min. Two of the samples (Set 1) were subjected to this procedure only.

Formation of Anodic Aluminium Oxide (AAO) layers: After undergoing the above-described preliminary treatment, some of samples have been subjected to galvanostatic anodization for 15 min in a 15 wt.% aqueous solution of H₂SO₄ with applied current density of 15 mAcm⁻² at 20°C. After anodizing, two samples were separated from the rest and were labeled as (Set 2).

Cerium Conversion Coating deposition: The electroless deposition was performed for 5 min in an electrolyte for ceria deposition, having the following composition: 0.025 M CeCl₃·7H₂O combined with 0.025 M (NH₄)₂Ce(NO₃)₆·4H₂O. Just prior to the coating depositions, 5 ml of 30% H₂O₂ (for each 250 ml of electrolyte) were added.

This process was carried out at two temperatures (at 20°C and at 50°C, respectively), on AA2024-T3 samples, with and without preliminary anodization. These CeCC deposition temperatures were selected, since they correspond to the temperatures of the preliminary desmutting, the anodizing (20°C) and the etching (50°C). To systematically evaluate the impact of the described procedures on the surface characteristics of the specimens, they were categorized into the following sets for comparative purposes: Set 1 - only preliminary treated; Set 2 - anodized after preliminary treatment; Set 3 - CeCC deposited at 20°C; Set 4 - CeCC layers formed at 50°C; Sets 5 and 6 - Combined AAO/CeCC

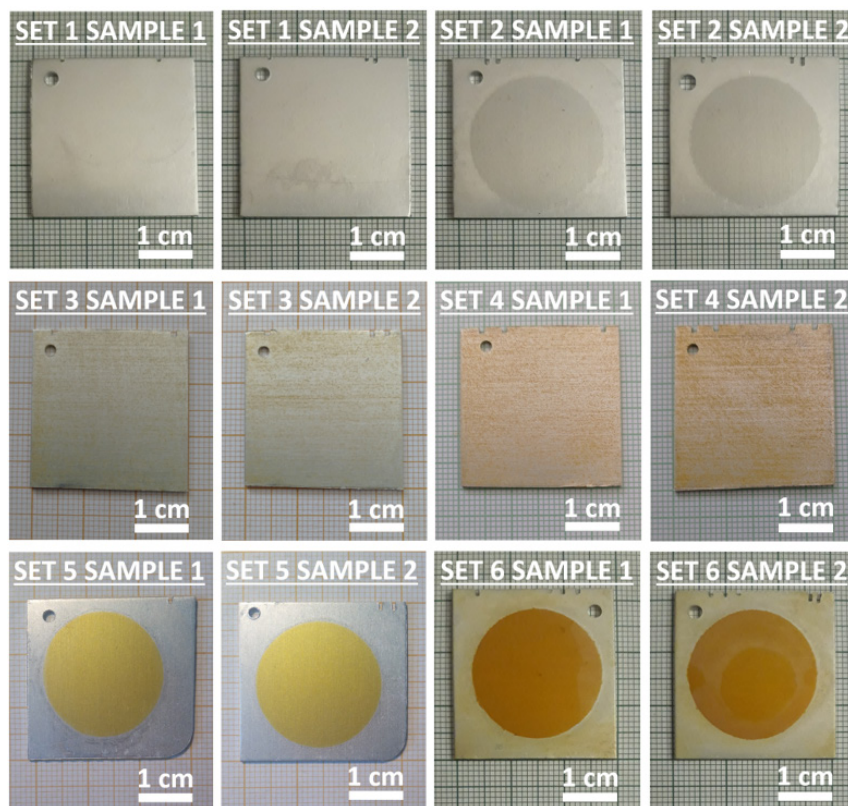


Fig. 1. Photographs of the investigated samples.

layers, formed by ceria formation at 20 or 50°C, after anodization. As depicted in Fig. 1, each set comprised a pair of representatives.

Characterization techniques

The investigations were organized in such a way as to obtain systematic data suitable for comparative research. As already mentioned, the measurement techniques were divided into two types: (i) determination of surface properties, and (ii) topology characterization.

Colour characteristics acquisition: The colour parameters of all samples were acquired using a RT 100 Lovibond tintometer. The obtained data are interpreted in the CIE (L*a*b*) colour space. Measurements were performed on 4 different sites of the surface of each sample, adding to a total of 8 points from each sample type. The aim was to determine the repeatability and detect any colour variations.

Wettability tests: The contact angle measurements were performed using a high-precision optical device “Theta Lite”, a product of Biolin Scientific (UK),

coupled with specialized software “One attention” (Finland). The constant volume of the drops was ensured using a “Gastight 1001” precise screw syringe, product of Hamilton Co. (USA). Analogically, the measurements were performed on 4 points on the surface of each sample (acquiring 8 measurements from each pair of samples, as mentioned above). The wettability of the samples is represented by the values of the angle between the water drops and the sample surfaces, θ° .

The results obtained by the statistical analyses of the data from the colour measurements and the wettability tests are presented in the form of $(MV_{av} \pm \Delta Y)$, where MV_{av} is the average value of the respective parameter obtained using the following equation:

$$MV_{av} = \frac{\sum MV_n}{n} \quad (1)$$

In this equation, MV_n are the directly measured values from the lowest value (MV_1) to the highest (MV_n); n is the number of measurements for the respective pair of samples (in the present research paper $n = 8$).

The confidential range constrains (ΔY) were calculated based on the standard deviations (s_n) using the following expression:

$$\Delta Y = \frac{\sum s_n t_{(for\ selected\ P\ and\ (n-1))}}{\sqrt{n}} \quad (2)$$

For the present research activities, the value of the student's criterion is chosen to be $t = 5.041$, which corresponds to $n = 8$ measurements and a probability of $P = 0.1\%$.

The sum of the standard deviations (Σs_n) is calculated by applying the following equation:

$$\sum s_n = \sqrt{\frac{(s_1^2 + \dots + s_n^2)}{n-1}} \quad (3)$$

The standard deviation (Σs_n) values for the respective measured quantity are defined as the difference between the respective value (MV_n , where $n = 1 \div 8$) and the mean value MV_{av} of a given parameter for the respective pair of samples.

Optical Metallographic Microscopy (OMM): These observations were carried out to observe the surface of the films. Optical micrographs with a resolution 640x480 were obtained at 100x magnification by a Boeco optical microscope equipped with PK-710G, product of A4Tech.

Scanning Electron Microscopy: The respective observations were performed on bare AAO layers and on deposited at the two temperatures CeCC layers. The equipment used is Sigma 560 VP, a product of Zeiss (Germany). Surface images were obtained at low (2500x) and high (10 000x) magnification rates, appointed as LM and HM in the respective figure, while these of the cross-sections - at 12 000x.

RESULTS AND DISCUSSION

Colour characteristics acquisition

The research activities for the present work began with systematic determination of the surface properties of all samples. The collected raw data from the colour and wettability measurements were submitted to statistical analysis. The student's criterion value was selected to be $t = 5.041$, for 8 results for each set, acquired by four measurements of two samples, as commented above. The statistically treated data are summarized in Table 1.

According to the brightness parameter L^* , all samples appear rather bright. Anodization results in slight darkening from $L^* \approx 97$ (for Set 1) to $L^* \approx 90$ (for Set 2), because of the increase in roughness due to the formation of a porous AAO layer. For comparison, the spontaneous CeCC deposition at 20°C (Set 3) practically does not affect the value of this parameter (it remains $L^* \approx 97$ for both Sets 1 and 3). This suggests that the coating does not cover the entire metal surface, and the typical metallic lustre is reflected through the uncovered areas. The CeCC deposition at 50°C leads to negligible darkening, down to $L^* \approx 89$ (Set 4). This fact is rather a result of the higher temperature of the CeCC formation, which probably results in predominance of Ce(IV) compounds formation.

As anticipated, the combination between AAO and CeCC leads to slightly more intense darkening: to $L^* \approx 84$ for CeCC deposited at 20°C (Set 5) and $L^* \approx 81$ for the layer deposited at 50°C (Set 6).

According to the green/red vector (a^*), the applied procedures convert the colour hue from insignificant reddish (with $a^* \approx 0.60$ for Set 1) to negligibly greenish (with $a^* \approx -0.65$ for Set 2). Most probably, the Cu-containing intermetallics react to form the greenish

Table 1. Statistically treated data for the surface characteristics of the samples after different treatment procedures.

Sample set	L^*	a^*	b^*	$\theta [^\circ]$
Set 1	97.10 ± 3.22	0.60 ± 0.05	2.47 ± 2.53	62.30 ± 30.51
Set 2	90.32 ± 1.76	-0.65 ± 0.79	2.27 ± 2.90	33.13 ± 5.36
Set 3	97.02 ± 3.12	-2.37 ± 0.59	14.81 ± 1.19	116.25 ± 24.18
Set 4	89.79 ± 2.74	-1.62 ± 0.46	23.39 ± 8.17	124.65 ± 16.98
Set 5	84.52 ± 2.66	-1.50 ± 0.95	59.01 ± 2.06	32.04 ± 12.98
Set 6	81.58 ± 1.21	-1.87 ± 3.53	62.58 ± 9.13	53.56 ± 9.66

Cu(OH)₂ during the coating formation procedures. The strongest effect is observed when the CeCC is deposited (Sets 3 and 4). The reason for the weaker variation of the parameter a^* after anodization is that this process causes partial dissolution of the intermetallics, as established in a previous work [13].

The most notable alteration is in the parameter b^* (the blue/yellow vector): from $b^* \approx 2.5$ for the references (Set 1) and the AAO layer (Set 2), its values increase to $b^* \approx 14$ and $b^* \approx 23$ for the directly deposited CeCC layers at 20°C (Set 3) and at 50°C (Set 4), respectively. Its values sharply rise to around and above $b^* \approx 60$ for the CeCC layers, deposited on preliminary anodized surfaces (Sets 5 and 6). This increase indicates that these coatings have a better coverage of the AAO layer, compared to this of bare metallic AA2024 surface.

Wettability tests

The measurements of the contact angle, θ (Table 1) reveal that the respective surface treatments lead to a rather noticeable change in surface hydrophobicity. The direct CeCC depositions on the preliminary treated A2024-T3 surface (Sets 3 and 4) transform its properties from relatively hydrophilic, with $\theta \approx 62^\circ$ (measured for Set 1) to absolutely hydrophobic with around and above $\theta \approx 120^\circ$, after the CeCC depositions at 20°C (Set 3) and at 50°C (Set 4). Such a change of hydrophobicity has already been mentioned in the literature [36, 37], as Liu et al. [38] attributed this effect to the formation of Ce-oxide/hydroxide structures with a defined micro-nano flower-like topology. In the present case, the hydrophobic coatings did not show superhydrophobicity, as water droplets were retained on the samples' surfaces. Hence, the directly deposited CeCC layers do not completely cover the metal surface, and the droplets are retained on the bare metal areas.

On the contrary, anodization leads to a decrease of the contact angle to $\theta \approx 33^\circ$. Thus, the surface of the AAO layers (Set 2) appears hydrophilic. The probable causes for this effect are related to the modification of the surface's texture, retention of anodizing electrolyte inside the pores or hydration of the AAO layer surface by $Al_2O_{3-x}(OH)_x$ compounds, such as boehmite, etc. However, the detailed investigation of these processes is not among the main objectives of the present research.

Finally, it should be mentioned, that the subsequent CeCC formation on the AAO layers at 20°C (Set 5) has

no effect on the value of the contact angle, while a slight increase in this parameter, up to $\theta \approx 55^\circ$, is observed for the combined CeCC/AAO layers formed at 50°C (Set 6). This effect can be explained by considering that after removing the coated samples from the bath at 50 °C, enhanced evaporation from their surface occurs due to the increased temperature.

Optical Metallographic Microscopy (OMM)

The optical metallographic microscopy (OMM) images, shown in Fig. 2, confirm that the colours of both types of samples, after the preliminary treatments (Set 1) and anodization (Set 2) are bright grey, whereas the direct CeCC layers are yellow (Set 3, formed at 20°C) or yellow with pronounced reddish tonality (Set 4, formed at 50°C). Furthermore, the CeCC layers deposited at 50°C appear to have relatively higher coverage compared to those formed at 20°C.

The combined CeCC/AAO layers reveal complete coverage of the sample surface by the conversion layer. This fact is a consequence of the highly textured Al_2O_3 film formed by the anodizing. Further, the surfaces of these samples (Sets 5 and 6) appear smoother than those of Sets 3 and 4.

Furthermore, the anodization induces partial dissolution of the intermetallics, suppressing the preferential "island-like" deposition on their surfaces described by some authors [39, 40]. Therefore, both effects of the anodization process contribute to the formation of a smooth and uniform CeCC layer. The CeCC deposition at 50°C on the AAO surfaces renders an additional beneficial effect. In this manner, the highly-textured surface of the AAO layer predetermines the formation of a uniform CeCC layer, which completely covers the anodized part of the sample's surface. This fact can be seen from the photographs in Fig. 1, in the experimental part.

In contrast, direct CeCC deposition without preliminary anodization resulted in sparse deposits (Sets 3 and 4 in Figs. 1 and 2), rather than dense, uniform ceria layers (Sets 5 and 6 in the same figures).

Scanning Electron Microscopy

Additional surface and cross-sectional SEM micrographs of the deposited layers were obtained to acquire more detailed information regarding the samples' topology and layer thickness. The acquired

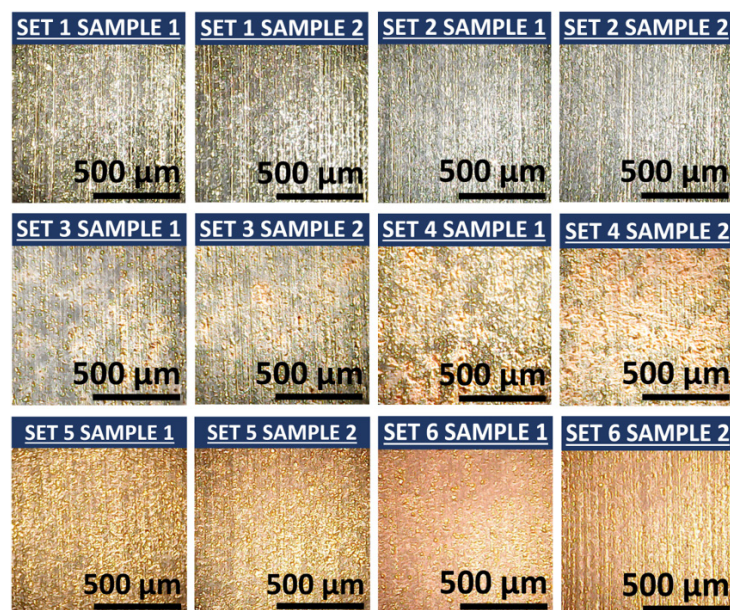


Fig. 2. Optical micrographs of AA2024-T3 specimens after different surface treatment procedures.

low- and high magnification images are presented in Fig. 3.

The surface topologies of the AAO layer and the AAO/CeCC layer, deposited at 20 °C reveal the typical surface topology, observed after the preliminary treatment, since it is known that the anodic film follows the metallic surface [41 - 43]. Numerous shallow craters are observed, formed due to accelerated dissolution of the alloy matrix around the cathodic intermetallics, described in detail by various authors [44 - 49].

The AAO/CeCC layer formed at 50°C reveals a highly cracked surface due to the thermal shock immediately after the sample is withdrawn from the bath. The film on the surface of the sample heated to 50°C undergoes intense dehydration due to the evaporation of water from the solution. At the same time, the metal substrate shrinks due to cooling, causing additional tensile stress on the newly formed CeCC coating. Undoubtedly, the cold-water wash applied immediately after the final CeCC deposition further contributes to the cracking of the film (under these conditions, the samples are subjected to increased thermal stress because the water temperature is lower than the room temperature).

The SEM observations of the AAO/CeCC layer formed at 50°C reveal a more interesting topology at higher magnifications. An image obtained at a 70 000x

magnification is presented in Fig. 4.

The surface topology reveals complete coverage of the AAO surface by agglomerates forming the CeCC layer. These agglomerates consist of hydrated globular cerium oxides and hydroxides, similar to the reference CeCC layers (i.e., the unsealed ones) described in other reports [50-52], with an average globule diameter of about 100 nm. Consequently, the respective markers in Fig. 4 show diameters varying from 84.14 to 135.40 nm.

Finally, cross sectional SEM images of the AAO layer, and the AAO/CeCC layers, formed at the two temperatures (20°C and 50°C) were acquired. These images are shown in Fig. 5.

As it can be seen from the image, all the films have about 5 μm thickness, due to the performed anodization. This thickness corresponds to the thickness of the AAO film obtained for 12 min under identical conditions [53 - 55].

Conceptual summary

Summarizing all the analysed data from the present research, it can be concluded that preliminary anodization leads to the formation of a uniformly distributed CeCC layer that completely covers the formed AAO layer. Furthermore, the CeCC layer was found to possess a morphology of aggregated globular nanoparticles with

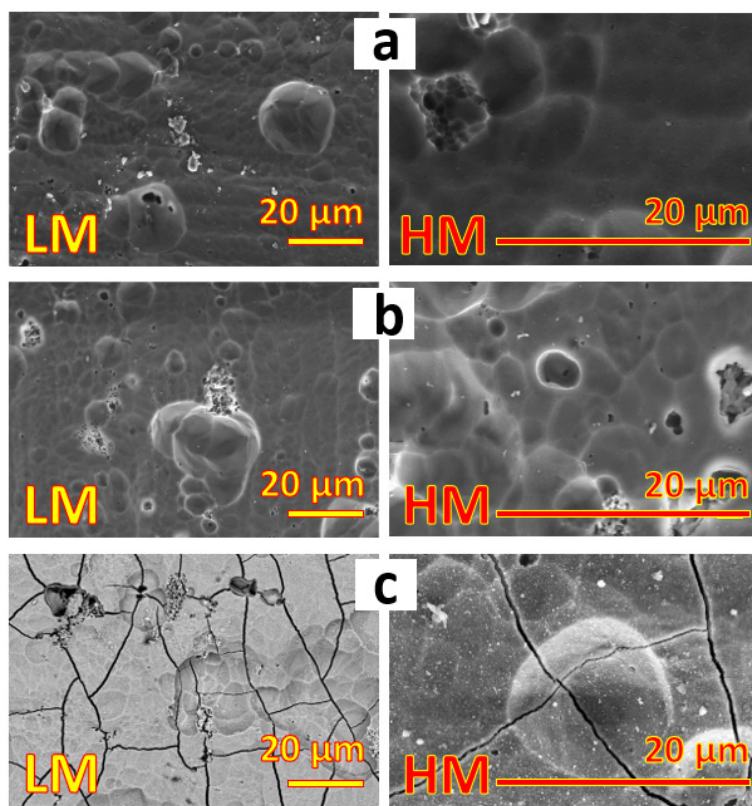


Fig. 3. Low (LM) and high (HM) magnification topological SEM images: (a) AAO layer, AAO/CeCC layer formed at (b) 20°C and (c) 50°C.

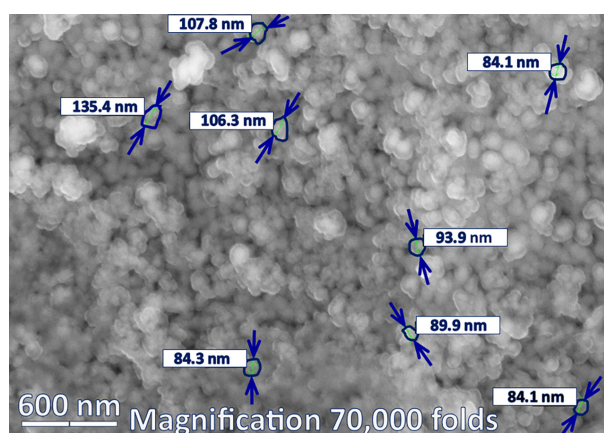


Fig. 4. SEM image of the AAO/CeCC layer formed at 50°C acquired at higher magnification.

an average diameter of about 100 μm , resembling the advanced CeCC layer reported by Selegard et al. [31]. Furthermore, an obvious synergism is obtained between the CeCC and AAO layers, resulting in a durable coating primer with a much-improved barrier ability. Both CeCC deposition approaches with and without preliminary anodization are illustrated in Fig. 6.

The illustration shows the advantage of depositing

a CeCC film on a preliminary formed AAO layer, comparing it to direct CeCC formation. The latter approach does not result in formation of uniform and dense layer, but rather in sparse, randomly distributed ceria-based deposits. The CeCC layer, in turn, seals the AAO layer pores, enhancing its corrosion-protective characteristics, as discussed in the Part I of the present study [56]. This synergism between the two layers results

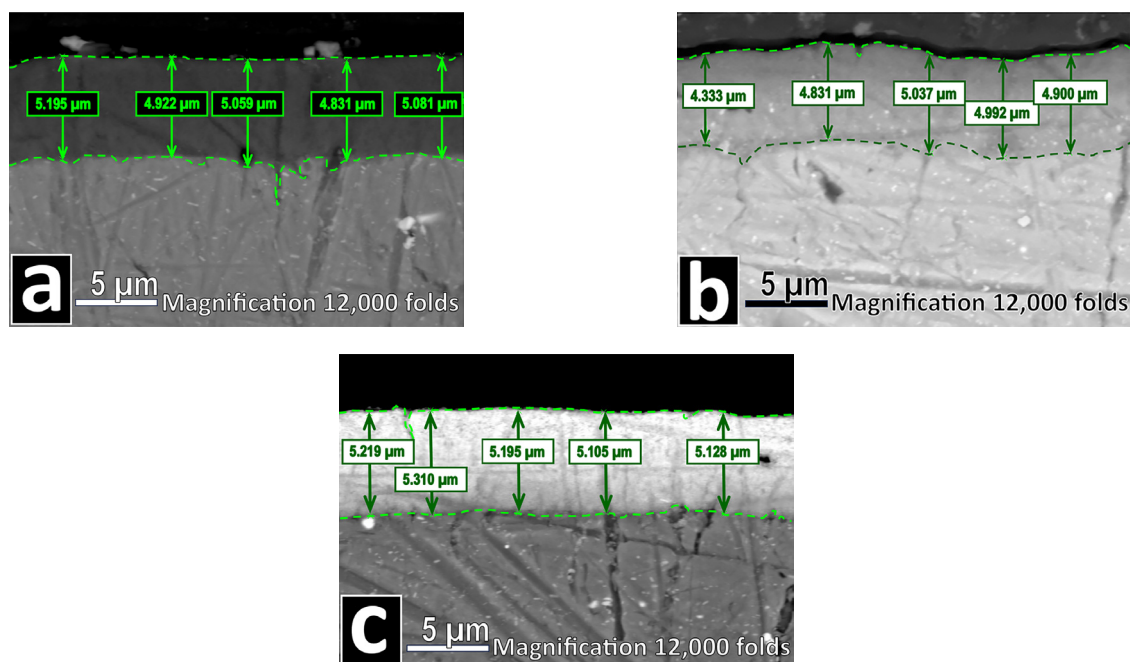


Fig. 5. Cross-sectional SEM images of the investigated samples: (a) AAO layer, AAO/CeCC layer deposited at (b) 20°C and (c) 50°C.

in the formation of a reliable and durable AAO/CeCC combined coating primer.

The photographs in Fig. 1 combined with the OMM images in Fig. 2 undoubtedly confirm this inference. In addition, the SEM images in Figs. 3, 4 and 5 reveal the uniform coverage and thickness of the combined AAO/CeCC layers.

Finally, the systematic electrochemical measurements further confirm the preference of anodization prior to CeCC deposition at both temperatures.

CONCLUSIONS

The present study is a part of systematic research activities, dedicated to the application of rare earth elements for the elaboration of reliable and durable coating primers. The impact of the cerium conversion coating on the surface characteristics of AA2024-T3 alloy samples with and without preliminary anodization was consistently evaluated. For completeness, the CeCC layers were deposited at two different temperatures.

The properties of the samples' coatings were also systematically characterized. The surface characterization techniques included preliminary colour and wettability analysis, combined with description of their topology

and further determination of electrochemical properties. The colour and contact angle data were subjected to statistical analysis.

The main findings of the present systematic study can be summarized as follows:

Anodization proceeds in a somewhat different way from the theoretical curves, described in the literature. The curves reach an almost constant voltage: about 17 V during the entire anodization periods. Initial short-term plateaus are observed at 5 V, probably due to the dissolution of the alloy's intermetallics.

The colour characteristics show a slight darkening due to the formation of the porous AAO layer. The direct formation of CeCC does not change the surface brightness, while the combination of these procedures results in more noticeable darkening. Moreover, the CeCC deposition results in a yellowish tonality, further enhanced by the preliminary anodization. This means that the combined AAO/CeCC layers completely cover the samples, unlike the directly deposited CeCC. This fact was the first evidence for the synergism between anodization and the deposition of the conversion coating. Obviously, the highly textured surface of the AAO layer predetermines the formation of a uniform CeCC layer, which completely covers the surface of the anodized sample.

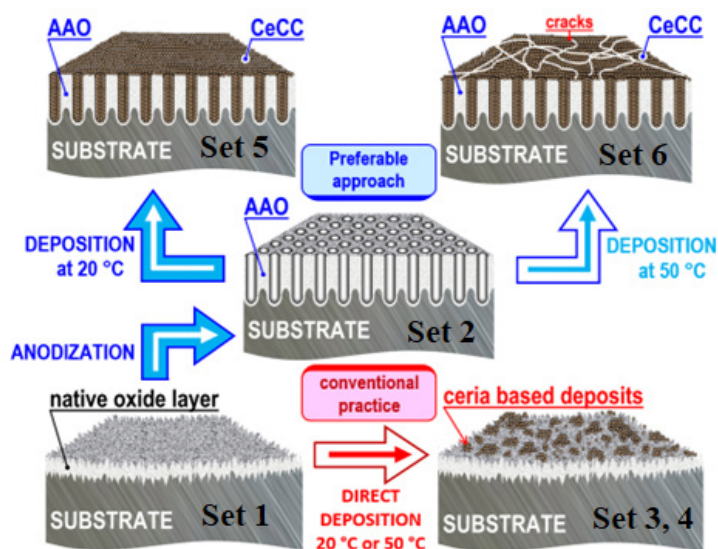


Fig. 6. Illustration of the approaches for CeCC deposition, applied in the present research.

From the Optical (OMM) microscopy images is evident that the surfaces of the samples are completely covered by the combined AAO/CeCC conversion layers. This is a consequence of the highly textured Al_2O_3 surface, formed by the anodization.

The surface topologies of the AAO layers and the AAO/CeCC layers, deposited at room temperature have shown a multitude of shallow craters, formed due to the accelerated alloy matrix dissolution around the cathodic intermetallics.

The AAO/CeCC layer, formed at 50°C has a strongly cracked surface, due to the thermal shock immediately after the withdrawal of sample from the bath. At higher magnifications, the surface topology has revealed the complete coverage of the AAO surface by CeCC layer agglomerates, composed by hydrated globular cerium oxides and hydroxides with an average globule diameter of about 100 nm.

The cross-sectional SEM images have shown that the thickness of all the observed samples is about 5 μm , due to the anodization process.

In conclusion, a clear synergism is observed between the AAO and CeCC layers, leading to the elaboration of reliable and durable combined AAO/CeCC coating primers that provide complete coverage of the substrate surface.

Acknowledgements

The authors express their gratitude for the financial backing of this research provided under Project No. KII-06-H79/1, titled "Protective and functional layers on aluminium and its alloys", supported by the Bulgarian National Science Fund. INFRAMAT, distributed research infrastructure of the National Roadmap for Scientific Infrastructure is acknowledged as well.

Authors's contributions: S.P.: Methodology, Formal Analysis, Investigation, Data Curation; S.K.: Conceptualization, Methodology, Data Curation, Writing, Original Draft, Visualization, Formal Analysis, Ch.G.: Writing, Review, Editing, Visualization, Data Curation, Methodology, Formal Analysis, Resources; V.L.: Formal Analysis, Data Curation, P.P.: Resources.

REFERENCES

1. R. Abdel-Karim, S.M. El-Raghy, in: Jean Ebothé, Waqar Ahmed (Eds.), Nanofabrication using Nanomaterials, One Central Press, Manchester, UK, 2016, pp. 197-218.
2. Ch.A. Girginov, S.V. Kozhukharov, in: Anton Hermansen (Ed.), Aluminium oxide, NOVA Sci.

- Publ., 2020, pp. 3-108.
3. W. Stepniowski, J.M. Salerno, in: W. Ahmed, N. Ali (Eds.), *Manufacturing Nanostructures*, One Central Press (OCP), Manchester (UK), 2014, pp. 321-357.
 4. W.J. Stepniowski, *Nanostructured Anodic Oxides: Fabrication and Applications*, *Curr. Nanosci.*, 15, 1, 2018, 3-5. <https://doi.org/10.2174/157341371501181205103558>
 5. G.D. Sulka, in: A. Eftekhari (Ed.) *Nanostructured Materials in Electrochemistry*, Wiley-VCH Verlag, 2008, pp. 1-116. <https://doi.org/10.1002/9783527621507.ch1>
 6. G. Patemarakis, P. Lenas, C.H. Karavassilis, G. Papayiannis, Kinetics of growth of porous anodic Al₂O₃ films on Al metal, *Electrochim. Acta*, 36, 3/4, 1991, 709-725. [https://doi.org/10.1016/0013-4686\(91\)85162-Z](https://doi.org/10.1016/0013-4686(91)85162-Z)
 7. G. Patemarakis, K. Moussoutzanis, Mathematical Models for the Anodization Conditions and Structural Features of Porous Anodic Al₂O₃ Films on Aluminum, *J. Electrochem. Soc.*, 142, 3, 1995, 737-743. <https://doi.org/10.1149/1.2048527>
 8. L. Zaraska, E. Wierzbicka, E. Kurowska-Tabor, G.D. Sulka, in: D. Losic, A. Santos (Eds.), *Nanoporous Alumina*, Springer Series in Materials Science, 219, 2015, 61-106. https://doi.org/10.1007/978-3-319-20334-8_3
 9. C.V. Manzano, D. Ramos, L. Pethö, G. Bürki, J. Michler, L. Philippe, Controlling the Color and Effective Refractive Index of Metal-Anodic Aluminum Oxide (AAO)-Al Nanostructures: Morphology of AAO, *J. Phys. Chem. C*, 122, 1, 2018, 957-963. <https://doi.org/10.1021/acs.jpcc.7b11131>
 10. F.A. Bruera, G.R. Kramer, M.L. Vera, A.E. Ares, Evaluation of the influence of synthesis conditions on the morphology of nanostructured anodic aluminum oxide coatings on Al 1050, *Surf. Interfaces*, 18, 2020, 100448. <https://doi.org/10.1016/j.surf.2020.100448>
 11. V. Rizkia, J.W. Soedarsono, B. Munir, B. Suharno, An analysis of the electrolyte resistivity effect on the pore diameter and pore density of anodic aluminium oxide (AAO) films produced by single-step anodization, *Int. J. Technol.* 8, 2017, 1479-1488. <https://doi.org/10.14716/ijtech.v8i8.742>
 12. F. Le Coz, L. Arurault, R. S. Bes, Simulation of The Electrical Transient During The Porous Anodizing Of Pure Aluminium Substrate, *WIT Trans. Eng. Sci.*, 54, 2007, 1-10. <https://doi.org/10.2495/ECOR070161>
 13. Ch. Girginov, S. Kozhukharov, M. Milanese, M. Machkova, Impact of the anodizing duration on the surface morphology and performance of A2024-T3 in a model corrosive medium, *Mater. Chem. Phys.*, 198, 2017, 137-144. <https://doi.org/10.1016/j.matchemphys.2017.05.049>
 14. M. Michalska-Domańska, W.J. Stepniowski, L.R. Jaroszewicz, Characterization of nanopores arrangement of anodic alumina layers synthesized on low-(AA1050) and high-purity aluminum by two-step anodizing in sulfuric acid with addition of ethylene glycol at low temperature, *J. Porous Mater.*, 24, 2017, 779-786. <https://doi.org/10.1007/s10934-016-0316-7>
 15. L. González-Rovira, L. González-Souto, P.J. Astola, C. Bravo-Benítez, F.J. Botana, Assessment of the corrosion resistance of self-ordered anodic aluminum oxide (AAO) obtained in tartaric-sulfuric acid (TSA), *Surf. Coat. Technol.*, 399, 2020, 126131. <https://doi.org/10.1016/j.surfcoat.2020.126131>
 16. A. Ruiz-Clavijo, O. Caballero-Calero, M. Martín-González, Revisiting anodic alumina templates: from fabrication to applications, *Nanoscale*, 13, 2021, 2227-2265. <https://doi.org/10.1039/d0nr07582e>
 17. M.P. Martínez-Viademonte, S.T. Abrahami, T. Hack, M. Burchardt, H. Terryn, A Review on Anodizing of Aerospace Aluminum Alloys for Corrosion Protection, *Coatings*, 10, 11, 2020, 1106. <https://doi.org/10.3390/coatings10111106>
 18. S. Kozhukharov, Ch. Girginov, in: P. Petkov, M. Achour, C. Popov (Eds.), *NATO Science for Peace and Security Series B: Physics and Biophysics*, Springer, Dordrecht (Netherlands), 2020, pp. 437-445. https://doi.org/10.1007/978-94-024-2018-0_35
 19. F. Presuel-Moreno, M.A. Jakab, N. Tailleart, M. Goldman, J.R. Scully, Corrosion-resistant metallic coatings, *Mater. Today*, 11, 2008, 14-23. [https://doi.org/10.1016/S1369-7021\(08\)70203-7](https://doi.org/10.1016/S1369-7021(08)70203-7)
 20. B.R.W. Hinton, D.R. Arnott, N.E. Ryan, The inhibition of aluminium corrosion by cerium cations, *Metals Forum*, 7, 1984, 211-217.
 21. B. R. W. Hinton, D. R. Arnott, N. E. Ryan, Cerium conversion coating for the corrosion protection of aluminium, *Metals Forum*, 9, 1986, 162-173.
 22. A.J. Davenport, H.S. Isaacs, M.W. Kendig, X-Ray Absorption Study of Cerium in the Passive Film on

- Aluminum, *J. Electrochem. Soc.*, 136, 1989, 1837-1838. <https://doi.org/10.1149/1.2097040>
23. A.J. Davenport, H. S. Isaacs, M. W. Kendig, XANES investigation of the role of cerium compounds as corrosion inhibitors for aluminum, *Corros. Sci.*, 32, 5-6, 1991, 653-663. [https://doi.org/10.1016/0010-938X\(91\)90113-4](https://doi.org/10.1016/0010-938X(91)90113-4)
24. F. Mansfeld, Y. Wang, H. Shih, The Ce-Mo process for the development of a stainless aluminum, *Electrochim. Acta*, 37, 12, 1992, 2277-2282. [https://doi.org/10.1016/0013-4686\(92\)85123-3](https://doi.org/10.1016/0013-4686(92)85123-3)
25. F. Mansfeld, Y. Wang, Development of "stainless" aluminum alloys by surface modification, *Mater. Sci. Eng., A*, 198, 1-2, 1995, 51-61. [https://doi.org/10.1016/0921-5093\(95\)80058-3](https://doi.org/10.1016/0921-5093(95)80058-3)
26. A.J. Aldykiewicz, A.J. Davenport, H.S. Isaacs, Studies of the Formation of Cerium-Rich Protective Films Using X-Ray Absorption Near-Edge Spectroscopy and Rotating Disk Electrode Methods, *J. Electrochem. Soc.*, 143, 1996, 147-154. <https://doi.org/10.1149/1.1836400>
27. M. Bethencourt, F.J. Botana, J.J. Calvino, M. Marcos, M.A. Rodriguez-Chacon, Lanthanide compounds as environmentally-friendly corrosion inhibitors of aluminium alloys: a review, *Corros. Sci.*, 40, 1998, 1803-1819. [https://doi.org/10.1016/S0010-938X\(98\)00077-8](https://doi.org/10.1016/S0010-938X(98)00077-8)
28. K.A. Yasakau, M.L. Zheludkevich, S.V. Lamaka, M.G.S. Ferreira, Mechanism of corrosion inhibition of AA2024 by rare-earth compounds, *J. Phys. Chem. B*, 110, 2006, 5515-5528. <https://doi.org/10.1021/jp0560664>
29. A. Conde, M.A. Arenas, A. De Frutos, J. de Damborenea, Effective corrosion protection of 8090 alloy by cerium conversion coatings, *Electrochim. Acta*, 53, 2008, 7760-7768. <https://doi.org/10.1016/j.electacta.2008.05.039>
30. L.E.M. Palomino, I.V. Aoki, H.G. de Melo, Microstructural and electrochemical characterization of Ce conversion layers formed on Al alloy 2024-T3 covered with Cu-rich smut, *Electrochim. Acta*, 51, 2006, 5943-5953. <https://doi.org/10.1016/j.electacta.2006.03.036>
31. L. Selegård, T. Poot, P. Eriksson, J. Palisaitis, P.O.Å. Persson, Z. Hu, K. Uvdal, In-situ growth of cerium nanoparticles for chrome-free, corrosion resistant anodic coatings, *Surf. Coat. Technol.*, 410, 2021, 126958. <https://doi.org/10.1016/j.surfcoat.2021.126958>
32. R. Andreeva, A. Tsanev, D. Stoychev, Effect of pre- and post-treatment operations of aluminum alloy Al-1050 protected by ceria conversion coatings, *Materials Today: Proceedings*, 61, 2022, 1280-1286. <https://doi.org/10.1016/j.matpr.2022.03.716>
33. R. Andreeva, A. Tsanev, D. Stoychev, Improving the Corrosion Resistance of Anodized Al 1050 Alloy by Sealing in Cerium-Containing and Mixed Sodium Phosphate Mono Basic and Calcium Nitrate Solutions, *Metals*, 14, 7, 2024, 768. <https://doi.org/10.3390/met14070768>
34. A. de Frutos, M.A. Arenas, Y. Liu, P. Skeldon, G.E. Thompson, J. de Damborenea, A. Conde, Influence of pre-treatments in cerium conversion treatment of AA2024-T3 and 7075-T6 alloys, *Surf. Coat. Technol.*, 202, 16, 2008, 3797-3807. <https://doi.org/10.1016/j.surfcoat.2008.01.027>
35. W. Pinc, S. Geng, M. O'Keefe, W. Fahrenholtz, T. O'Keefe, Effects of acid and alkaline based surface preparations on spray deposited cerium based conversion coatings on Al 2024-T3, *Appl. Surf. Sci.*, 255, 2009, 4061-4065. <https://doi.org/10.1016/j.apsusc.2008.10.110>
36. C.E. Castano, M.J. O'Keefe, W.G. Fahrenholtz, Cerium-based oxide coatings, *Curr. Opin. Solid State Mater. Sci.*, 19, 2015, 69-76. <https://doi.org/10.1016/j.cossms.2014.11.005>
37. J. Liang, Y. Hu, Y. Fan, H. Chen, Formation of superhydrophobic cerium oxide surfaces on aluminum substrate and its corrosion resistance properties, *Surf. Interface Anal.*, 45, 8, 2013, 1211-1216. <https://doi.org/10.1002/sia.5255>
38. C. Liu, F. Su, J. Liang, P. Huang, Facile fabrication of superhydrophobic cerium coating with micro-nano flower-like structure and excellent corrosion resistance, *Surf. Coat. Technol.*, 258, 2014, 580-586. <https://doi.org/10.1016/j.surfcoat.2014.08.032>
39. T. Zehra, M. Kaseem, Lanthanides: the key to durable and sustainable corrosion protection, *ACS Sustainable Chem. Eng.*, 2023, 11, 18, 6776-6800. <https://doi.org/10.1021/acssuschemeng.3c00763>
40. M.A.A. Khan, O.M. Irfan, F. Djavanroodi, M. Asad, Development of Sustainable Inhibitors for Corrosion Control, *Sustainability*, 14, 15, 2022, 9502. <https://doi.org/10.3390/su14159502>

41. E.A. Matter, S.V. Kozhukharov, M.S. Machkova, Effect of the preliminary treatment on the superficial morphology and the corrosion behaviour of AA2024-T3 aluminum alloy, *Bulg. Chem. Commun.*, 43, 1, 2011, 23-30.
42. E. Matter, S. Kozhukharov, M. Machkova, V. Kozhukharov, Reproducibility of the corrosion parameters for AA2024-T3 aluminium alloy after different preliminary treatment procedures, *J. Chem. Technol. Metall.*, 50, 1, 2015, 52-64.
43. E. Matter, S. Kozhukharov, Correlation between preliminary pretreatments and the behaviour of AA-2024 - aluminium alloy in 3.5% NaCl model corrosive medium, *Ann. Proceeds, Univ. Rousse (Bulgaria)*, 49, 9.1, 2010, 14-19. <https://conf.uniruse.bg/bg/docs/cp10/9.1/9.1-2.pdf>
44. H. Ju, S. Liu, W. Zhang, Y. Yang, J. Duan, Investigation of pitting corrosion and hydrogen evolution of aluminum and AA2024 alloy by simultaneous electrochemical measurements and imaging, *Electrochem. Commun.*, 132, 2021, 107135. <https://doi.org/10.1016/j.elecom.2021.107135>
45. X. Zhang, X. Zhou, T. Hashimoto, B. Liu, Localized corrosion in AA2024-T351 aluminium alloy: Transition from intergranular corrosion to crystallographic pitting, *Mater. Charact.*, 130, 2017, 230-236. <https://doi.org/10.1016/j.matchar.2017.06.022>
46. F.M. Queiroz, M. Terada, A.F.S. Bugarin, H. Gomes de Melo, I. Costa, Comparison of Corrosion Resistance of the AA2524-T3 and the AA2024-T3, *Metals*, 11, 6, 2021, 980. <https://doi.org/10.3390/met11060980>
47. P. Klomjit, P. Khamsuk, E. Viyanit, Root cause analysis of pitting corrosion of AA2024 and AA7075 after exposure in salt fog environment, *Int. J. Surf. Sci. Eng.* 15, 1, 2021, 18-35. <https://doi.org/10.1504/IJSURFSE.2021.10037021>
48. P. Rodič, I. Milošev, G.S. Frankel, Corrosion of Synthetic Intermetallic Compounds and AA7075-T6 in Dilute Harrison's Solution and Inhibition by Cerium(III) Salts, *J. Electrochem. Soc.*, 170, 3, 2023, 031503. <https://doi.org/10.1149/1945-7111/acc0a3>
49. Z. Wang, P. Chen, H. Li, B. Fang, R. Song, Z. Zheng, The intergranular corrosion susceptibility of 2024 Al alloy during re-ageing after solution treating and cold-rolling, *Corros. Sci.*, 114, 2017, 156-168. <https://doi.org/10.1016/j.corsci.2016.11.013>
50. R. Andreeva, A. Tsanev, D. Stoychev, Formation of environmentally friendly protective Ce₂O₃-CeO₂ conversion coatings on Al, modified by phosphate layers: chemical and electrochemical characterization, *Bulg. Chem. Commun.*, 55, 4, 2023, 390-406.
51. A. Tsanev, R. Andreeva, D. Stoychev, Influence of the Chemical Composition of Ceria Conversion Coatings, Sealed in Solution of NaH₂PO₄ and Ca(NO₃)₂, on the Corrosion Behavior of Aluminum, *Materials* 16, 19, 2023, 6499, 1-21. <https://doi.org/10.3390/ma16196499>
52. Ch. Girginov, S. Portolesi, S. Kozhukharov, A. Tsanev, E. Lilov, P. Petkov, Selection of appropriate electrochemical deposition regime for cerium conversion coating on anodized AA2024-T3 aircraft alloy, *J. Appl. Electrochem.*, 54, 2024, 1171-1202. <https://doi.org/10.1007/s10800-023-02012-9>
53. Ch. Girginov, S. Kozhukharov, M. Milanec, M. Machkova, Impact of the anodizing duration on the surface morphology and performance of A2024-T3 in a model corrosive medium, *Mater. Chem. Phys.*, 198, 2017, 137-144. <https://doi.org/10.1016/j.matchemphys.2017.05.049>
54. S. Kozhukharov, Ch. Girginov, S. Portolesi, A. Tsanev, V. Lilova, P. Petkov, Optimal current density for cathodic CeCC deposition on anodized AA2024-T3 aircraft alloy, *J. Appl. Electrochem.*, 54, 2024, 2887-2918. <https://doi.org/10.1007/s10800-024-02143-7>
55. S.V. Kozhukharov, Ch. Girginov, S. Portolesi, A. Tsanev, V. Lilova, M. Georgieva, E. Lilov, Sealing of cerium oxide coating primers on anodized AA2024-T3 alloy by boiling in Lourier buffers, *J. Electrochem. Sci. Eng.*, 14, 5, 2024, 559-582. <http://dx.doi.org/10.5599/jese.1949>
56. S. Portolesi, Ch. Girginov, S. Kozhukharov, V. Lilova P. Petkov, A. Tsaneva, Enhancing surface characteristics of AA2024-T3 aircraft alloy through synergistic anodization and cerium conversion coating. Part I: Performance in model corrosive medium, *J. Chem. Technol. Metall.*, 59, 6, 2024, 1289-1304, DOI:10.59957/jctm.v59.i6.2024.3